ACS Catalysis

Research Article

pubs.acs.org/acscatalysis

# Ruthenium Phosphide Synthesis and Electroactivity toward Oxygen Reduction in Acid Solutions

Hanan Teller,[†] Olga Krichevski,[†] Meital Gur,[†] Aharon Gedanken,[‡] and Alex Schechter*[,†]

[†]Department of Biological Chemistry, Ariel University, Ariel 40700, Israel

[‡]Department of Chemistry, Bar-Ilan University, Ramat-Gan 52902, Israel

Supporting Information

**ABSTRACT:** Ruthenium phosphides are known to be highly stable and conductive materials. A new process was developed to prepare ruthenium phosphide catalysts for oxygen reduction in acid solutions. Several synthesis methods have been applied to form pure RuP and $Ru_2P$ as well as mixed phases of Ru and $Ru_xP$ ($x \geq 1$). These methods utilize high-temperature solid-state synthesis and reaction under autogenic pressure at elevated temperature (RAPET). On the basis of rotating ring−disk electrode (RRDE) experiments, oxygen reduction activity was observed on all $Ru_xP$ materials. Characteristic kinetic parameters show specific exchange current densities in the range of 0.4−1.4 mA $mg^{-1}$, Tafel slopes of 129−135 mV $dec^{-1}$, and $\%H_2O_2$ of 3−11% of the total current. Complementary XPS and Raman spectral analysis reveals a highly oxidized surface with significant presence of $PO_4^{3-}$ and $RuO_2$ species. To the best of our knowledge, this is the first report identifying oxygen reduction activity on $Ru_xP$.

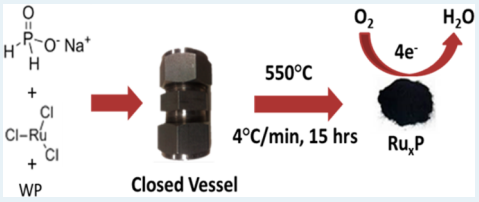


**KEYWORDS:** *RuP, $Ru_2P$, ruthenium, phosphide, preparation, catalyst, oxygen, reduction*

## 1. INTRODUCTION

The electrochemical oxygen reduction reaction (ORR) to water has been intensely investigated due to its importance in many practical applications. Specifically, the ORR plays a key role in electrochemical energy conversion devices such as metal−air batteries and fuel cells.[1−3] The most widely studied catalysts in fuel cell cathodes are Pt[4,5] and Pt alloys,[6] on which the reduction reaction occurs mostly via an overall four-electron mechanism.[7] Nevertheless, the high cost of Pt and its limited durability in acid solutions are the major barriers in the way of fuel cell commercialization. Different classes of Pt free catalysts have been studied over the last few decades. Among the most promising stable catalysts for ORR in acid solution are ruthenium-based compounds.

Ruthenium metal was reported as a limited activity ORR catalyst in acid and alkaline solutions. More recently, ruthenium-based transition-metal chalcogenides were studied for ORR. Ternary and binary Ru chalcogenides, such as $Mo_{6-x}Ru_xL_y$[8] and $Ru_xL_y$ where L = Se,[9] S,[10] Te,[11] have been reported. Few of these catalysts show high electroactivity toward oxygen reduction and tolerance to methanol contamination. $Ru_xSe_y$ species exhibit the best performance in these respects. Although the ORR mechanism on these catalysts remains unclear, several studies have been published. Tributsh et al. have suggested that surface selenous species and Ru−Se complexes present at different oxidation states reduce the kinetic barriers for oxygen reduction and result in the favored four-electron reduction directly to water. This reaction requirement for two adjacent vacant Ru sites is disturbed by the presence of a high surface concentration of Se.[12] The role of chalcogenides on the coordination number of ruthenium sites was explored by Alonso-Vante. It was shown by an in situ EXAFS study that dissociative adsorption of oxygen onto the $Ru_xSe_y$ active centers favors the four-electron mechanism reaction.[11] Chalcogen atoms modify and stabilize Ru surfaces by inhibiting the formation of $RuO_2$, which is claimed to be inactive in the ORR.[13,14]

Recently Mukerjee et. al suggested that oxygen can be adsorbed both on the oxide-free Ru surface and on ruthenium oxide or hydrated ruthenium. The adsorption on metallic ruthenium leads to direct reduction to $H_2O$ via a 4e process, while reduction over hydrated oxide and hydroxide groups Ru layers leads mainly to 2e reduction to $H_2O_2$, due to an outer-sphere reaction imposed by the lower electronic conductivity through these layers.[15]

Density functional theory (DFT) calculations were performed by Tritsaris et al. to study the oxygen reduction on selenium- and sulfur-containing transition-metal surfaces, including ruthenium.[16] The authors found a linear relationship between the d band of the surface metal atoms and the adsorption energies of the ORR intermediates, in support of a direct link between the reactivity of the surface and its electronic structure. Interestingly, RuP and RuAs follow the same trend as RuSe and RuS. Nevertheless, no prior experimental work on RuP as oxygen reduction catalysts could be found.

Metal−phosphide materials are used in the fields of supercapacitors and catalysis.[17,18] There are only a few

Received: December 29, 2014
Revised: May 28, 2015
Published: June 1, 2015





DOI: 10.1021/acscatal.5b00880
ACS Catal. 2015, 5, 4260−4267

known methods of preparing phosphides, which include high-temperature reduction of phosphate and pyrophosphate salts by hydrogen at 800−1000 °C to produce MoP, WP, $Fe_2P$, $Ni_2P$, FeP, and RuP,[19] high-temperature treatment of organometallic precursors,[20] and reactions with phosphines or organic phosphines (e.g., trioctylphosphine).[21,22]

RuP materials show high stability in acid solutions and higher electronic conductivity in comparison to Ru carbides and nitrides.[23] However, the synthesis of these materials is problematic and is based on the reaction of Ru salt with phosphine gas, which is highly toxic. Amorphous RuP foils were grown by CVD on $SiO_2$ from *cis*-$H_2Ru(PMe_3)_4$ (Me = $CH_3$) as the single precursor at temperatures of 250−300 °C. XPS measurements showed the presence of elemental Ru and P with no precise stoichiometry.[24] Recently there have been reports on the synthesis of RuP powders with stoichiometries of 2/1 and 1/1, by a solid-state reaction of $RuCl_3$ and hypophosphite.[23,25] We hereby report the investigation of novel synthesis methods to produce $Ru_xP$ ($x \geq 1$) and the study of their electrocatalytic activity toward oxygen reduction in acid solutions.

## 2. EXPERIMENTAL SECTION

**2.1. Synthesis of Ru−P Materials.** Several methods were employed in the syntheses of Ru−P compounds.

*2.1.1. Synthesis S1: Solid-State Reaction in Open Vessel.* A 0.430 g portion of $NaH_2PO_2$ (4.9 mmol) and 0.504 g of $RuCl_3$ (2.45 mmol) were dissolved in deionized water, forming a P:Ru molar ratio of 2:1. After heat drying, the powder was heat-treated at 550 °C for 1 h.

*2.1.2. Synthesis S2: Liquid-Phase Reaction in Closed Vessel.* A 0.12 g portion of red phosphorus (3.87 mmol) was heated under an $N_2$ atmosphere to obtain white phosphorus (WP), followed by an addition of 5 mL of DI water and a 10 mL solution of 0.506 g of $NaH_2PO_2$ (5.75 mmol), 0.3 g of $RuCl_3$ (1.45 mmol), and 0.06 g of sodium dodecyl sulfate (SDS) (0.21 mM). The molar ratio of white phosphorus to $NaH_2PO_2$ and to $RuCl_3$ was 2.7:4.0:1.0, respectively. The mixture was sealed in a 23 mL Swagelok union connector and annealed at 180 °C for 15 h. Identical syntheses were repeated excluding WP (synthesis S2a) and SDS (synthesis S2b).

*2.1.3. Synthesis S3: Reaction under Autogenic Pressure at Elevated Temperature (RAPET).* This technique, which was previously reported in the synthesis of various nanostructured materials, utilizes the high pressure formed during the reaction at elevated temperatures inside a stainless steel reactor, to produce RuP under a hermetically sealed atmosphere. The reaction takes place under the internal pressure evolving in the reactor during the reaction.[26,27] In this study, 0.3 g of $NaH_2PO_2$ (3.40 mmol) and 0.28 g of $RuCl_3$ (1.35 mmol) were dissolved in water and dried to give a P:Ru molar ratio of 1:2.5, respectively. The mixture was sealed and heated at 550 °C for 1 h.

**2.2. Characterization Techniques.** Transmission electron microscopy (TEM) measurements were performed using a JEOL-JEM-1000SX system. Scanning electron microscopy (SEM) and Energy dispersive X-ray spectrometry (EDS) measurements were performed using a JEOL-6510LV microscope. The crystal structure analysis was carried out by a Philips X'Pert X-ray diffractometer with Cu K$\alpha$ radiation source. XPS analysis was performed in a Kratos AXIS-HS spectrometer, using a monochromated Al K$\alpha$ source. All XPS measurements were carried out at room temperature, under a vacuum of (1.0−3.0) × $10^{-9}$ Torr. Raman spectra were recorded with a XploRA ONE micro-Raman system (Horiba Scientific, France) using 530 nm laser, power <150 mW.

Electrochemical measurements were performed in a standard three-electrode glass cell equipped with Pt-wire counter electrode and Ag/AgCl (Metrohm) reference electrode. The working electrode was a 5 mm diameter glassy-carbon disk surrounded by a Pt concentric ring (PINE instruments). Active material, RuP catalyst, was deposited on the center disk from a homogeneous suspension consisting of catalyst powder, Nafion solution (15 wt %, ion power), XC72 carbon black (15 wt %, Cabot) for unsupported catalyst, and water/isopropyl alcohol solution. A 5 $\mu$L drop of this slurry was spread on the disk electrode and dried to give a final catalyst loading of 50 $\mu g/cm^2$. This working electrode was attached to a rotator (MSRX, Pine Instruments) in RRDE and RDE measurements in 0.5 M $H_2SO_4$ saturated with pure nitrogen or oxygen, using CHInstruments 700C and 760C Bipotentiostats.

## 3. RESULTS AND DISCUSSION

**3.1. Materials Preparation and Characterizations.** *3.1.1. $Ru_2P$ Characterization.* Samples S1 and S2 in Table 1 were characterized by EDS and XRD measurements. Figure 1 shows the X-ray diffraction pattern of S1, where the main peaks were detected at 38.15° (112), 38.37° (210), and 40.62° (211), attributed to various orthorhombic $Ru_2P$ *hkl* values.[28] Notably, no sign of reactant residuals, ruthenium oxides or phosphates,

**Table 1. Summary of Synthesis Techniques, Ru:P Molar Ratios in Precursors and Products (EDX), and Surface Compositions (XPS)**

| sample | synth method | temp (°C) | Ru:P in precursors | product | XPS |
|---|---|---|---|---|---|
| S1 | open vessel solid state | 550 | 1:2 | $Ru_2P$ | $Ru_2P$, 52% O |
| S2 | closed vessel liquid stat | 180 | 1:6.7 | $Ru_2P$ + Ru | |
| S2a | (S2), no WP | 180 | 1:4 | 90% Ru + 10% P | |
| S2b | (S2), no SDS | 180 | 1:6.7 | $Ru_2P$ | $Ru_2P$, 66% O |
| S3 | RAPET | 550 | 1:2.5 | RuP | RuP, 55% O |

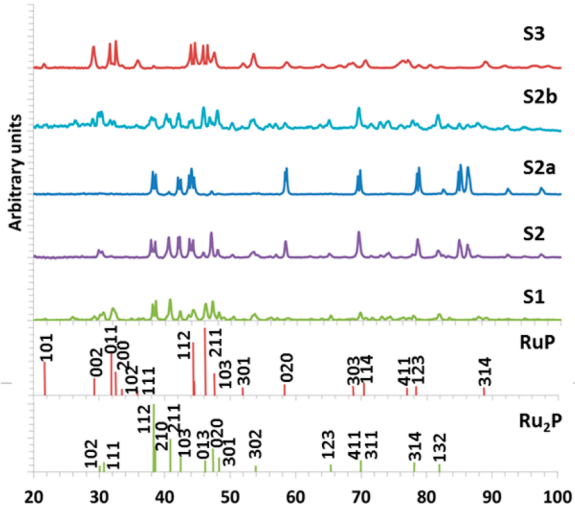


**Figure 1.** XRD patterns of Ru−P materials synthesized by solid state in open vessel (S1), liquid phase in sealed vessel (S2, S2a, and S2b), and RAPET (S3) techniques.



DOI: 10.1021/acscatal.5b00880
*ACS Catal.* 2015, 5, 4260−4267

other RuP structures, or Ru can be identified in this bulk powder diffraction pattern. Samples prepared by the low-temperature procedure produced powders with Ru:P atomic ratios of 1:3, 1:9, and 2:1 assigned to S2, S2a, and S2b, respectively, on the basis of EDX measurements. XRD analysis of these three products revealed an amorphous structure. Upon annealing at 700 °C for 2.5 h under $N_2$, $Ru_2P$ + Ru mixed phases, as well as elemental Ru and P, were attained in addition to $Ru_2P$ from products S2, S2a, and S2b, respectively.

TEM micrographs of $Ru_2P$ prepared by the S1 method in Figure 2a display a network structure having a mean diameter

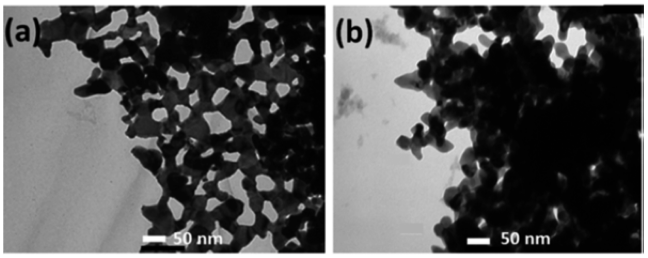


**Figure 2.** TEM images of (a) $Ru_2P$ synthesized by solid state reaction in open vessel (S1) and (b) RuP synthesized by RAPET technique (S3).

of 50 nm, whereas the size of the observed particles in the SEM is characterized by large aggregates (up to 25 $\mu$m) comprised of small nanometric particles (not shown). The SEM image of particles formed in the S2 synthesis in Figure 3 presents highly spherical particles with diameters ranging from 300 to 850 nm.

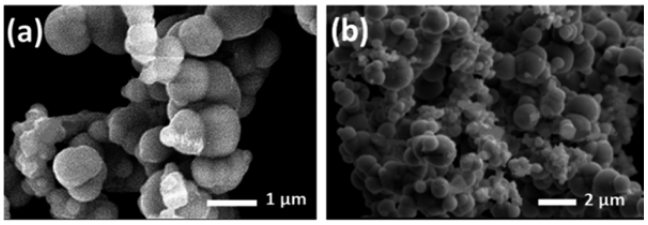


**Figure 3.** SEM micrographs of liquid phase (S2) in sealed vessel synthesis products (a) before and (b) after annealing at 700 °C for 2.5 h.

X-ray photoelectron spectroscopy (XPS) of S1 $Ru_2P$ was used to analyze the surface composition of these particles. Although ruthenium is typically analyzed in XPS by following the strong signals from the 3d photoelectrons, here we used the 3p spectra instead, in order to avoid interferences from the carbon tape substrate.

The calculated signals of Ru 3p and P 3p shown in Figure 4a,b give an atomic ratio of 2:1 Ru:P, in agreement with the XRD and the EDS measurements of the bulk material. According to Figure 4b, the spectrum of Ru 3p shows at least two Ru peaks. The Ru $3p_{3/2}$ main peak at 462 eV is rather broad and can be referenced to several compounds including Ru, $Ru_xP$, and $RuO_x$ (462.2 eV),[29] whereas the peaks at higher binding energies are attributed to oxidized RuP species (e.g., $RuPO_4$) and RuOH (464.1 eV).[29] The oxygen atomic surface concentration in these samples was 52% (Table 1), which constitutes an almost completely oxidized surface. Theoretically, a fully oxidized surface of $Ru_2P$ (to $RuO_2$ and $RuPO_4$) is expected to provide an oxygen concentration of 66.7%.

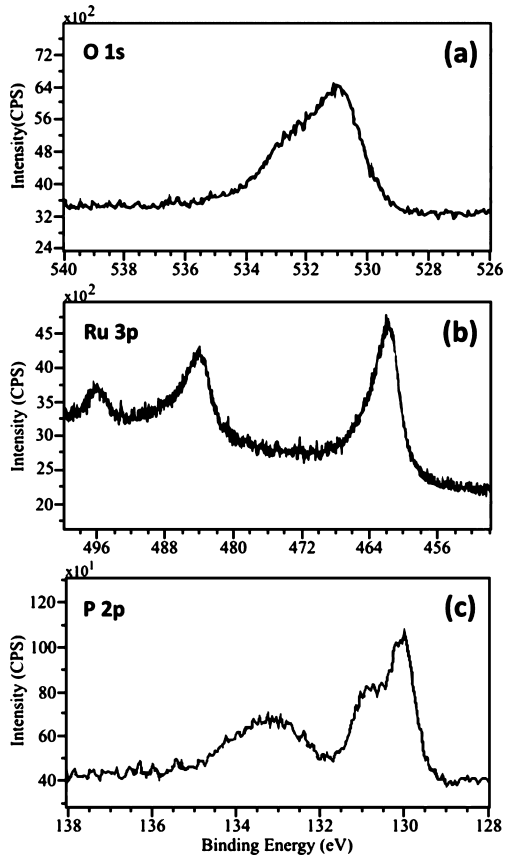


**Figure 4.** XPS measurements of $Ru_2P$ synthesized by solid state reaction in open vessel (S1): (a) O 1s; (b) Ru 3p; (c) P 2p.

The analysis of the O 1s spectrum in Figure 4a shows a broad signal with a maximum at 531 eV and a shoulder at 533 eV, which can be attributed to highly oxidized Ru and P molecules (e.g., $P_2O_5$,[30] $RuPO_4$ (based on 531.8 eV for $FePO_4$[31]), and $RuO_2$ (531.6 eV)).[32] At least three peaks of phosphorus can be observed in the P 2p spectrum in Figure 4c, at 130, 132, and 133.5 eV. While the low binding energy signals are attributed to an elemental P peak (130.9 eV),[33] lower binding energies correlate to negatively charged and highly oxidized surface P atoms: e.g. $RuPO_4$ (based on 133.7 eV for $FePO_4$[34]), respectively.

Raman spectroscopy measurements of the $Ru_2P$ particles, synthesized by closed vessel liquid state (S2b) and solid state reactions in an open vessel (S1), dispersed on a silicon wafer were collected in the range of 150−1250 $cm^{-1}$ (Figure 5). Peaks at that range are attributed to oxidized species of phosphorus and ruthenium. More specifically, the peaks at 175 and 340 $cm^{-1}$ were reported as $PO_4$,[35] whereas the peaks at 395, 1008, and 1100 $cm^{-1}$ were reported as phosphate and biphosphate ions.[36,37] The presence of $RuO_2$ on the surfaces was observed from the spectrum of Figure 5 at 468, 510, and 730 $cm^{-1}$.[38] Nevertheless, differences between the two presented spectra are clearly seen. The peaks at 730, 1008, and 1100 $cm^{-1}$ are missing from the S2b spectrum, whereas a new peak appears at 510 $cm^{-1}$ assigned to $RuO_2$ (001). These changes should be attributed to the synthetic routes of the S1 and S2b materials, resulting in various crystallites, reflected in the differences in the corresponding $Ru_2P$ XRD patterns (Figure 1) and leading to the formation of distinctive oxides.[38] In addition, the hydrolysis step applied in the formation of S2b



DOI: 10.1021/acscatal.5b00880
ACS Catal. 2015, 5, 4260−4267

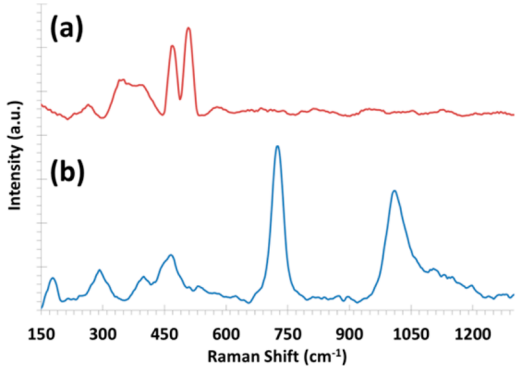


**Figure 5.** Raman spectra of $Ru_2P$ synthesized by (a) closed vessel liquid state (S2b) and (b) solid state reaction in an open vessel (S1).

may modify some of the surface phosphates. XPS measurements of the S2b sample showed a higher oxygen atomic concentration of 66%, which indicates an almost fully oxidized surface.

Further efforts were made to better understand the role of white phosphate (WP) and surfactant in this new low-temperature synthesis method, by performing the reaction in the absence of WP (designated as S2a) or SDS (synthesis S2b). XRD structural analysis of S2a displays only Ru crystallites with no evidence of known $Ru_xP_y$ species (Figure 1), and EDS of this product confirms the presence of only 10% P. When the S2 synthesis was repeated, this time in the presence of WP but without SDS surfactant (synthesis S2b), the resulting powder had irregular, nonspherical shape and an amorphous structure but had a Ru:P atomic ratio of 2:1. It is therefore concluded that the WP facilitates the low-temperature reaction, activated by $NaH_2PO_2$.[39] However, the SDS behaves as a templating agent, forming the Ru-containing spheres in Figure 2. It is likely that the SDS layer covering these particles passivates the surface of freshly formed $Ru_2P$, thus leading to incomplete reaction and to formation of two phases—$Ru_2P$ and Ru (synthesis S2 vs S2b).

*3.1.2. RuP Characterization.* The reaction under autogenic pressure at elevated temperature (RAPET) technique was applied using $NaH_2PO_2$ as the sole phosphorus precursor (synthesis S3). A selected $NaH_2PO_2$:$RuCl_3$ molar ratio of 2.5:1 yielded a product with an Ru:P atomic ratio of 1:1 (Table 1). TEM micrographs in Figure 2b show that small-size irregular particles of about 25 nm in diameter had been formed and aggregated into larger clusters. The structural XRD analysis depicted in Figure 1 is in agreement with a polycrystalline RuP pattern,[40] having various *hkl* orientations. Using a higher reactant ratio of 6:1 for $NaH_2PO_2$:$RuCl_3$ using this method yielded an nonuniform distribution of Ru and P content in the EDS mapping measurements, supported by XRD clearly exhibiting RuP and $Ru_2P$ mixed phases (not shown).

Table 1 summarizes the XPS, XRD, and EDS results of S3 RuP. The Ru:P atomic ratio in the bulk of these particles is very similar to that identified in the XPS surface analysis. A comparison to $Ru_2P$ shows very similar XPS spectra of RuP. The oxygen content reaches about 50% of the total atoms, in line with identified Raman oxide species.

We have noticed that reactions occurring at 550 °C (S1 and S3) required lower excess of $NaH_2PO_2$ to $RuCl_3$ in comparison to syntheses at low temperatures (S2, S2a, and S2b), which utilized ratios of 4−6.7.

In previous work by Li et al. the authors proposed a mechanism for $Ru_2P$ and RuP synthesis from $NaH_2PO_2$ and $RuCl_3$.[23] According to this mechanism, $Ru^{3+}$ is first reduced to $Ru^0$, which then reacts with $PH_3$ gas released from $NaH_2PO_2$ to form $Ru_2P$. The general equation for this reaction is

$$8RuCl_3 + 14NaH_2PO_2 \rightarrow 4Ru_2P + 9HCl + 3PCl_5 + 7Na_2HPO_4 + 6H_2\uparrow \quad (1)$$

$Ru_2P$ may further react with $PH_3$ to produce RuP via the equation

$$4Ru_2P + 2PH_3 \rightarrow 4RuP + 3H_2 \quad (2)$$

Hence, the overall reaction is given by

$$8RuCl_3 + 22NaH2PO_2 \rightarrow 9HCl + 3PCl_5 + 11Na_2HPO_4 + 8RuP + 12H_2\uparrow \quad (3)$$

The above reactions suggest that the required stoichiometric ratios of $RuCl_3$ to $NaH_2PO_2$ to yield $Ru_2P$ and RuP are 1.75 and 2.75, respectively. In practice, Li et al. were able to isolate pure $Ru_2P$ and RuP only when these ratios were 3.5 and 5.75, respectively.

However, in our study, employing the RAPET method (S3 product), RuP was produced at a $RuCl_3$:$NaH_2PO_2$ ratio of only 1:2.5. Formation of RuP at an apparent $NaH_2PO_2$ deficiency may be attributed to a parallel second mechanism in which $H_2$ gas, formed by reactions 1 and 2 in the closed vessel, reduce $RuPO_4$ formed in eq 4:

$$Na_2HPO_4 + RuCl_3 \rightarrow RuPO_4 + 2NaCl + HCl \quad (4)$$

$RuPO_4$ is inevitably formed from eq 1 by means of ion exchange. The resulting reaction can be described according to reaction 5:

$$RuPO_4 + 4H_2 \rightarrow RuP + 4H_2O \quad (5)$$

Reduction of ruthenium pyrophosphate to RuP + P under an $H_2$ stream at 600 °C was reported previously.[19] The authors also reported the reduction of $FePO_4$ to $Fe_2P$ in $H_2$ at 1000 °C.

**3.2. Catalytic Activity Study.** *3.2.1. Kinetic Permeates Identification.* Oxygen reduction reaction (ORR) kinetics was studied by linear sweep voltammetry (LSV), applied to a rotating ring−disk electrode (RRDE) and coated with RuP catalysts. The catalyzed central glassy-carbon disk was scanned in a potential range of 1.00 to 0.07 V vs SHE, while the Pt ring was held at a constant potential of 1.20 V (vs SHE). At this potential no significant $O_2$ reduction or water oxidation can occur. Thus, the total $O_2$ reduction current on the disk ($I_D$) is distinguished from the 2e reduction product of $H_2O_2$, oxidized on the ring ($I_R$).

Figure 6a depicts typical $I_D$ vs applied disk potential curves, measured from RuP (S3) at different electrode rotation speeds. All curves are characterized by an onset potential at 0.7 V (SHE) and a plateau limiting $O_2$ diffusion current that increases with the rotation speed. Interestingly, there is a change in the $I_D$ slope below 0.25 V, which becomes more noticeable above an electrode rotation speed of 200 rpm. Similar behavior is an indication of a mechanism change assigned to two separate oxygen active sites or adsorption energy on the same site.[41] This behavior is supported by the diversity of P and O surface species detected in our XPS and Raman results above.



DOI: 10.1021/acscatal.5b00880
*ACS Catal.* 2015, 5, 4260−4267

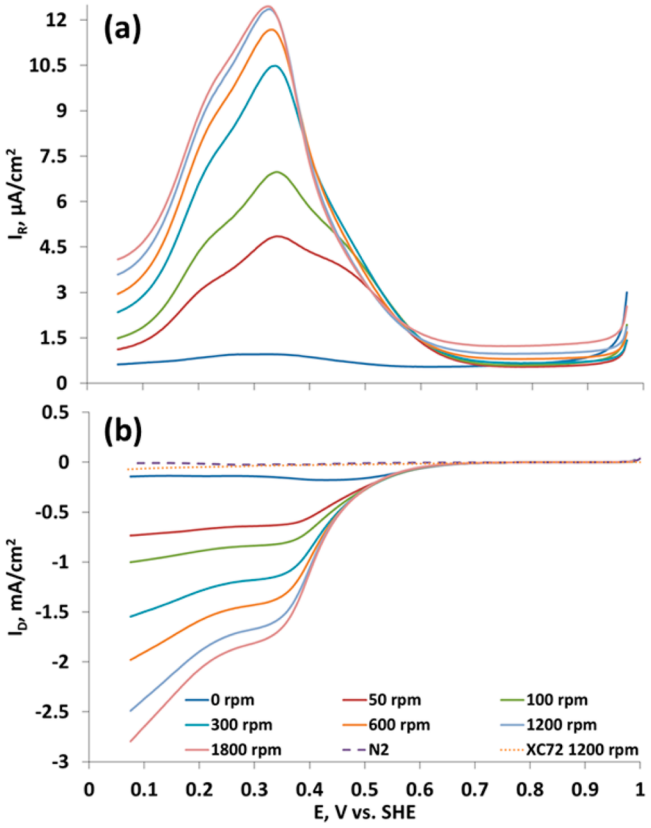


**Figure 6.** Current−potential curves for $O_2$ reduction on RuP RAPET S3 synthesized nanocatalysts: (a) ring; (b) disk. For comparison background current under $N_2$ and oxygen reduction on XC72 Vilkan carbon curves are included. Conditions: RRDE electrode in 0.5 M $H_2SO_4$ solution, scan rate 2 mV/s.

The ring current, ascribed to $H_2O_2$ oxidation, is plotted as a function of the disk potential in Figure 6b. It is significantly lower than the total ORR disk current, indicating that most of the ORR proceeds via the 4e path. $I_R$ follows the $I_D$ from the onset potential. Namely, $I_R$ rises with the overall current at 0.7 V and increases with the electrode rotation speed, suggesting that $H_2O_2$ formation is potential dependent, as seen in other ruthenium-based catalysts.[42] A maximum $H_2O_2$ production is observed as a broad peak at a disk potential of 0.3 V. Fast generation of $H_2O_2$ is dominant in the low overpotential region of 0.7−0.3 V. However, at potentials below 0.3 V the rate of peroxide formation decreases. In parallel to the disk second slope (Figure 6a), at around 0.2 V vs SHE, there is an additional small $I_R$ peak, which appears as a shoulder of the main peak (Figure 6b). Its presence is understood on the basis of having more than one active site of ruthenium, being activated at higher overpotentials (lower disk potentials). Apparently, this peak should be attributed to the second reduction process seen on the disk in Figure 5a and discussed above.

All of the materials that were synthesized and evaluated in this study show some electroactivity toward ORR. However, the onset overpotentials of ORR on these catalysts seem to be relatively high in comparison to those of other Ru-based catalysts such as $Ru_xSe_y$ and Pt. In order to evaluate the kinetic parameters governing the ORR on the prepared electrocatalysts in the study, the kinetic current ($i_k$) was calculated by using the Koutecky−Levich equation

$$\frac{1}{i} = \frac{1}{i_d} + \frac{1}{i_k} = \frac{1}{i_k} + \frac{1}{B\omega^{1/2}} \quad (6)$$

where $i_d$ is the diffusion limiting current which is a function of $\omega$, the angular velocity in radians $s^{-1}$, and $B = 0.62nFCD^{2/3}\nu^{-1/6}$, where $n$ is the overall number of electrons transferred in oxygen reduction, $F$ is the Faraday constant ($F$ = 96485 C $mol^{-1}$), $C$ is the bulk concentration of $O_2$ ($1.13 \times 10^{-6}$ mol $cm^{-3}$), $\nu$ is the kinematic viscosity of the electrolyte (0.01 $cm^2$ $s^{-1}$), and $D$ is the diffusion coefficient of $O_2$ ($1.8 \times 10^{-5}$ $cm^2$ $s^{-1}$).[43] Figure 7a shows the linear regression fitted line of the $1/i$ vs $1/\omega^{1/2}$ plot and the number of calculated transferred electrons $n$.

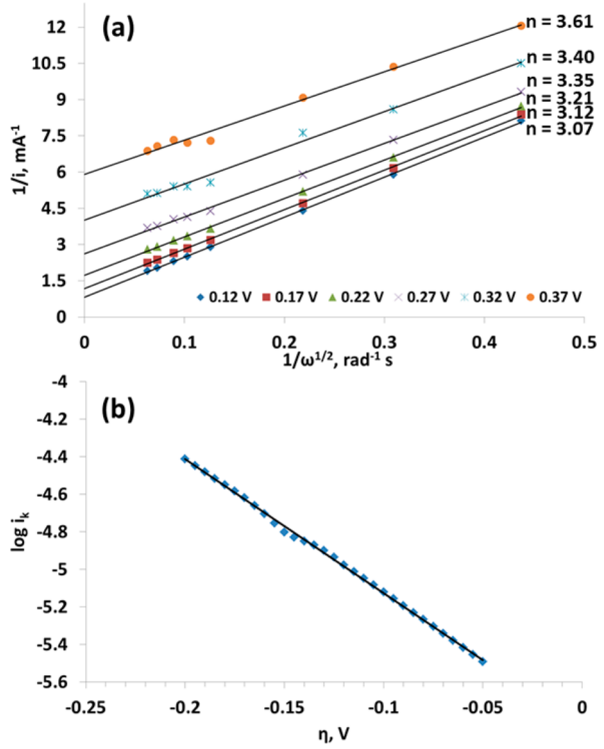


**Figure 7.** (a) $1/i$ vs $1/\omega^{1/2}$ plot with calculated number of electrons $n$ at different potentials and (b) log $i_k$ vs $\eta$ Tafel plot of the oxygen reduction reaction on $Ru_2P$ synthesized by solid state reaction in open vessel (S1).

$i_k$ was calculated from the intercept of the linear regression fitted line of $1/i$ vs $1/\omega^{1/2}$ plot at $\omega \rightarrow 0$ shown in Figure 7b. A collection of the kinetic currents at each selected potential provides the potential profile of pure activation controlled kinetic current, from which the Tafel slope $b$ and the exchange current density $i_0$ are calculated, by means of linear fitting of log $i_k$ vs $\eta$ (overpotential) shown in Figure 7b in accordance with the Tafel plot equation[44]

$$\log\ i = \log\ i_0 + b\eta \quad (7)$$

The calculated $b$ values of $Ru_2P$ and RuP prepared in this study are 135 and 129 mV/decade, respectively. These values are relatively high in comparison to that of Pt (60 mV/decade) and commercial Ru (101 mV/decade), measured under the same conditions. Interestingly, the exchange current density $i_0$ values for these synthesized materials, $1.4 \times 10^{-4}$ and $1.3 \times 10^{-4}$ A/mg, respectively, are considerably higher than that of Ru ($0.4 \times 10^{-4}$ A/mg), indicating that the density of free active sites on these catalysts is relatively high.



DOI: 10.1021/acscatal.5b00880
ACS Catal. 2015, 5, 4260−4267

It appears that the source of the apparent low electroactivity of the catalysts in the study in comparison to that of Pt and other Ru-based catalysts may be attributed to the high extent of oxidized species found on the particle surface, as shown in the XPS and Raman measurements presented in Table 1. The role of the oxide species layer on the surface of the catalyst particles was investigated by Mukerjee et al., who suggested that oxygen is adsorbed on the free Ru active surface sites as well as on OH and other oxide-containing ligands covering the outer surface layer of Ru. While direct oxygen reduction is expected from $O_2$ on metallic Ru sites in a charge transfer reaction mechanism, reduction on oxidized layers proceeds by an outer-sphere mechanism. In the latter case, the oxide surface area increases the electron transfer resistance, thus lowering the electroactivity of the catalyst.[15] The high extent of oxidized species on the Ru−P catalysts presented in this work is reflected in the high $b$ values and low $i_0$ values which result from the sluggish electron transfer through this oxidized layer. Therefore, the first electron transfer step ($O_2(ad) + e \rightarrow O_2^-(ad)$) is likely to be the rate-determining step of the oxygen reduction process.

The influence of various oxides detected on $Ru_2P$ prepared by closed vessel liquid state (S2b) and solid state reactions in open vessel (S1) on ORR was explored. A high onset reduction potential of 0.6 V (SHE) was measured in S2b, while the onset potential in S1 was 100 mV lower. This suggests that oxide species formed on $Ru_2P$ on S1 have lower charge transfer resistance and therefore are more effective in promoting ORR. The role of each type of surface oxide (e.g., $RuPO_4$ and $RuO_2$) on the $O_2$ reduction mechanism is yet to be revealed.

Reduction of the oxide layer was performed by temperature program reduction (TPR) of $Ru_2P$ under 5% $H_2$/95% Ar stream in the temperature range 150−800 °C at 20 °C/min. The reduced catalyst surfaces presented in RDE-LSV experiments a higher overpotential of 0.1 V and consequently lower ORR currents in comparison to freshly prepared $Ru_2P$. We attribute the observed lower kinetics to reoxidation of the reduced surface under oxygen during the experiment as well as to agglomeration of the particles at 800 °C.

**Table 2. $H_2O_2$ Yield Percentage during Oxygen Reduction Reaction on Ru−P Catalysts**

| | % $H_2O_2$ | |
|---|---|---|
| disk potential (V vs NHE) | sample S1 | sample S3 |
| 0.4 | 11.2 | 6.7 |
| 0.3 | 7.3 | 5.1 |
| 0.2 | 5.2 | 2.9 |

Table 2 shows the $H_2O_2$ production percentage at different potentials, which were calculated from the LSV/RRDE measurements results, using the equation

$$\%\ H_2O_2 = \frac{200(I_r/N)}{I_d + (I_r/N)} \quad (8)$$

where $I_r$ and $I_d$ are the ring and the disk currents, respectively, and $N$ is the electrode's collection coefficient.[45] All RuP materials have relatively high $H_2O_2$ percentage values in comparison to other Ru-based electrocatalysts, including $RuSe_x$.[46] The highest % $H_2O_2$ formation is ascribed to $Ru_2P$, 11.2%, while the lowest is for RuP, 6.4% at 0.4 V vs Ag/AgCl. At lower potentials of 0.2 V, the % $H_2O_2$ values of these catalysts further decrease to 5.7 and 2.9, respectively, most likely due to consecutive reduction of $H_2O_2$ to water on free Ru sites.

These relatively high values of % $H_2O_2$ in Table 2 are attributed to the highly oxidized catalytic surfaces which hinder charge transfer and therefore promote the two-electron reduction to $H_2O_2$ at the expense of a direct 4e mechanism.

*3.2.2. Methanol Tolerance.* Despite the superior electrocatalytic activity of Pt toward oxygen reduction, the use of it as the catalyst in direct methanol fuel cell cathodes is somewhat problematic due to the crossover of methanol from the anode side and the mixed potential effect associated with it.[47] Hence it is highly desirable to identify materials with high selectivity to $O_2$ reduction in the presence of methanol, regarded as methanol tolerance. Figure 8 shows the LSV of oxygen reduction on RuP in the presence and in the absence of 1 M methanol. The two voltammograms are nearly identical, evidence for the high tolerance of this catalyst toward methanol contamination.

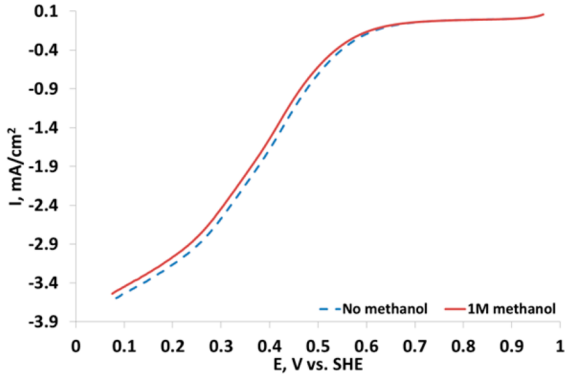


**Figure 8.** Current−potential curves for $O_2$ reduction on RuP RAPET S3 synthesized nanocatalyst in $O_2$ saturated 0.5 M $H_2SO_4$ solution in the presence and in the absence of 1 M methanol at 2 mV/s and 1800 rpm.

*3.2.3. Oxygen Reduction on Oxidized RuP.* In light of the important role of oxidized species on the RuP surface, it was advisable to verify this effect by further oxidizing the surfaces intentionally.

$Ru_2P$ electrodes were polarized to 1.12 V vs Ag/AgCl for 600 s in $O_2$-saturated 0.5 M $H_2SO_4$ solution. The effect of this electrochemical step is seen in Figure 9a. The voltammetric behavior of this electrode in $N_2$ prior to and after oxidation provides the following observations. The capacitive currents as well as surface redox waves of reduction at 0 V and oxidation at 0.4 V are significantly diminished. This is in support of passive oxide layer formation that increases interfacial resistance. It is important to note that unlike Pt catalysts, which also form oxide layers at potentials above 750 mV only to be reduced at lower potentials, oxidized RuP surfaces have not shown signs of oxide reduction even when they are polarized to negative potentials of −0.5 V where $H_2$ gas evolves.

The effect of this oxidized layer on oxygen reduction is seen through the LSV of an RRDE electrode at 1800 rpm before and after the treatment (Figure 9b). Formation of an oxide layer dramatically reduces the oxygen reduction current, due to interfacial resistance increase.


DOI: 10.1021/acscatal.5b00880
ACS Catal. 2015, 5, 4260−4267

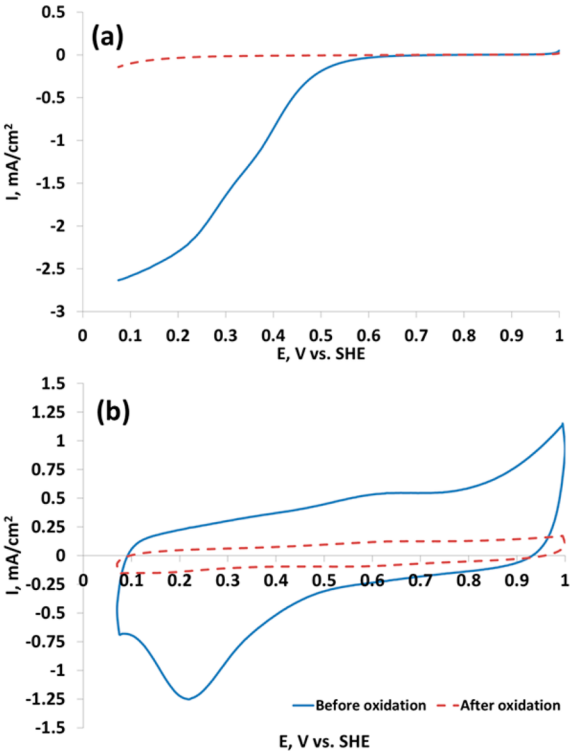


**Figure 9.** Current−potential curves for $Ru_2P$ electrode before and after oxidation: (a) $N_2$ saturated 0.5 M $H_2SO_4$ solution at 100 mV/s; (b) RDE in $O_2$ saturated 0.5 M $H_2SO_4$ solution at 2 mV/s and 1800 rpm.

## 4. CONCLUSIONS

For the first time we report the synthesis and oxygen reduction activity of $Ru_xP$ catalyst in acid solutions. Several novel synthetic routes were applied to prepare a variety of $Ru_xP$ ($x \geq 1$) materials, on the basis of solid and liquid phase synthesis and RAPET. Pure phases of RuP and $Ru_2P$ were produced using RAPET and open vessel solid state techniques, respectively, while low-temperature liquid state synthesis ended in amorphous product or a composite of Ru and $Ru_2P$ and their reactants.

RuP prepared at elevated temperatures of 550 °C yielded a metallic network of nanoparticles. Surface analysis by XPS and Raman revealed that the surface composition of these catalysts is largely occupied by oxidized species of ruthenium and phosphorus. This was suggested as the main reason for the observed limited electroactivity toward oxygen reduction. The adsorption of $O_2$ on the oxide-rich surface layer, which covers the catalysts and hinders the electronic charge transfer, is suggested as the main mechanism for the low ORR. It also gives rise to $H_2O_2$ formation via the less favored 2e mechanism, as reflected by the ring currents measured in RRDE experiments. Despite the relatively low electroactivity of these catalysts, their stability under acidic conditions and relatively high temperatures and their high tolerance toward methanol contamination demonstrated in this study make RuP and $Ru_2P$ good candidates as an active catalyst substrate in fuel cell electrodes.

## ■ ASSOCIATED CONTENT

### Supporting Information

The Supporting Information is available free of charge on the ACS Publications website at DOI: 10.1021/acscatal.5b00880.

XPS spectra of $Ru_2P$ (S1 and S2b) and RuP (S3) materials (PDF)

## ■ AUTHOR INFORMATION

### Corresponding Author

*A.S.: tel, 972-3937-1477; fax, 972-3907-6586; e-mail, salex@ariel.ac.il.

### Notes

The authors declare no competing financial interest.

## ■ ACKNOWLEDGMENTS

This work was supported by the Israel Science Foundation (ISF) through the Israel National Research Center for Electrochemical Propulsion (INREP) and I-CORE Program (number 2797/11)

## ■ REFERENCES

(1) Steele, B. C. H.; Heinzel, A. *Nature* **2001**, *414*, 345−352.
(2) Cheng, F.; Chen, J. *Chem. Soc. Rev.* **2012**, *41*, 2172−2192.
(3) Gattrell, M.; MacDougall, B. In *Handbook of Fuel Cells*; Vielstich, W., Lamm, A., Gasteiger, H. A., Eds.; Wiley: Chichester, U.K., 2005; Vol. *2*, pp 441−489.
(4) Gottesfeld, S. *ECS Trans.* **2008**, *6*, 51−67.
(5) Stephens, I. E. L.; Bondarenko, A. S.; Gronbjerg, U.; Rossmeisl, J.; Chorkendorff, I. *Energy Environ. Sci.* **2012**, *5*, 6744−6762.
(6) Wu, J.; Yang, H. *Acc. Chem. Res.* **2013**, *46*, 1848−1857.
(7) Anastasijević, N. A.; Vesović, V.; Adžić, R. R. *J. Electroanal. Chem. Interfacial Electrochem.* **1987**, *229*, 305−316.
(8) Sebastian, P. I.; Rodriguez, F. I.; Solorza, O.; Rivera, R. *J. New Mater. Electrochem. Syst.* **1999**, *2*, 115−119.
(9) Shukla, A. K.; Raman, R. K. *Annu. Rev. Mater. Res.* **2003**, *33*, 155−168.
(10) Reeve, R. W.; Christensen, P. A.; Dickinson, A. J.; Hamnett, A.; Scott, K. *Electrochim. Acta* **2000**, *45*, 4237−4250.
(11) Alonso-Vante, N.; Malakhov, I. V.; Nikitenko, S. G.; Savinova, E. R.; Kochubey, D. I. *Electrochim. Acta* **2002**, *47*, 3807−3814.
(12) Fiechter, S.; Dorbandt, I.; Bogdanoff, P.; Zehl, G.; Schulenburg, H.; Tributsch, H.; Bron, M.; Radnik, J.; Fieber-Erdmann, M. *J. Phys. Chem. C* **2006**, *111*, 477−487.
(13) Horkans, J.; Shafer, M. W. *J. Electrochem. Soc.* **1977**, *124*, 1202−1207.
(14) Anastasijević, N. A.; Dimitrijević, Z. M.; Adžić, R. R. *Electrochim. Acta* **1986**, *31*, 1125−1130.
(15) Ramaswamy, N.; Mukerjee, S. *Adv. Phys. Chem.* **2012**, *2012*, 1−17.
(16) Tritsaris, G. A.; Nørskov, J. K.; Rossmeisl, J. *Electrochim. Acta* **2011**, *56*, 9783−9788.
(17) Hirai, D.; Takayama, T.; Hashizume, D.; Takagi, H. *Phys. Rev. B: Condens. Matter Mater. Phys.* **2012**, *85*, 140509−140510.
(18) Reynal, A.; Lakadamyali, F.; Gross, M. A.; Reisner, E.; Durrant, J. R. *Energy Environ. Sci.* **2013**, *6*, 3291−3300.
(19) Gopalakrishnan, J.; Pandey, S.; Rangan, K. K. *Chem. Mater.* **1997**, *9*, 2113−2116.
(20) Stamm, K. L.; Garno, J. C.; Liu, G.-y.; Brock, S. L. *J. Am. Chem. Soc.* **2003**, *125*, 4038−4039.
(21) Yang, S.; Liang, C.; Prins, R. *J. Catal.* **2006**, *237*, 118−130.
(22) Qian, C.; Kim, F.; Ma, L.; Tsui, F.; Yang, P.; Liu, J. *J. Am. Chem. Soc.* **2004**, *126*, 1195−1198.
(23) Guan, Q.; Sun, C.; Li, R.; Li, W. *Catal. Commun.* **2011**, *14*, 114−117.
(24) Shin, J.; Waheed, A.; Agapiou, K.; Winkenwerder, W. A.; Kim, H.-W.; Jones, R. A.; Hwang, G. S.; Ekerdt, J. G. *J. Am. Chem. Soc.* **2006**, *128*, 16510−16511.
(25) Bowker, R. H.; Smith, M. C.; Pease, M. L.; Slenkamp, K. M.; Kovarik, L.; Bussell, M. E. *ACS Catal.* **2011**, *1*, 917−922.
(26) Pol, S. V.; Pol, V. G.; Frydman, A.; Churilov, G. N.; Gedanken, A. *J. Phys. Chem. B* **2005**, *109*, 9495−9498.



DOI: 10.1021/acscatal.5b00880
*ACS Catal.* 2015, 5, 4260−4267

(27) Pol, S. V.; Pol, V. G.; Kessler, V. G.; Seisenbaeva, G. A.; Solovyov, L. A.; Gedanken, A. *Inorg. Chem.* **2005**, *44*, 9938−9945.
(28) Rundqvist, S. *Acta Chem. Scand.* **1960**, *14*, 1961−1979.
(29) Wang, W.; Guo, S.; Lee, I.; Ahmed, K.; Zhong, J.; Favors, Z.; Zaera, F.; Ozkan, M.; Ozkan, C. S. *Sci. Rep.* **2014**, *4*, 1−9.
(30) Chowdari, B. V. R.; Tan, K. L.; Chia, W. T. *J. Non-Cryst. Solids* **1990**, *119*, 95−102.
(31) Barbaux, Y.; Dekiouk, M.; Le Maguer, D.; Gengembre, L.; Huchette, D.; Grimblot, J. *Appl. Catal., A* **1992**, *90*, 51−60.
(32) Shen, J. Y.; Adnot, A.; Kaliaguine, S. *Appl. Surf. Sci.* **1991**, *51*, 47−60.
(33) Pelavin, M.; Hendrickson, D. N.; Hollander, J. M.; Jolly, W. L. *J. Phys. Chem.* **1970**, *74*, 1116−1121.
(34) Franke, R.; Chassé, T.; Streubel, P.; Meisel, A. *J. Electron Spectrosc. Relat. Phenom.* **1991**, *56*, 381−388.
(35) Tominaga, Y.; Urabe, H.; Tokunaga, M. *Solid State Commun.* **1983**, *48*, 265−267.
(36) Niaura, G.; Jakubenas, R. *J. Electroanal. Chem.* **2001**, *510*, 50−58.
(37) Sauer, G. R.; Zunic, W. B.; Durig, J. R.; Wuthier, R. E. *Calcif. Tissue Int.* **1994**, *54*, 414−420.
(38) Korotcov, A. V.; Huang, Y.-S.; Tiong, K.-K.; Tsai, D.-S. *J. Raman Spectrosc.* **2007**, *38*, 737−749.
(39) Ni, Y.; Li, J.; Jin, L.; Xia, J.; Hong, J.; Liao, K. *New J. Chem.* **2009**, *33*, 2055−2059.
(40) Rundqvist, S. *Acta Chem. Scand.* **1962**, *16*, 287−292.
(41) Adzic, R. In *Electrocatalysis*; Ross, J. L. a. P. N., Ed.; Wiley-VCH: New York, 1998; pp 197−242.
(42) Lee, J.-W.; Popov, B. *J. Solid State Electrochem.* **2007**, *11*, 1355−1364.
(43) Gottesfeld, S.; Raistrick, I. D.; Srinivasan, S. *J. Electrochem. Soc.* **1987**, *134*, 1455−1462.
(44) Bard, A. J.; Faulkner, L. R. *Electrochemical methods Fundamentals and Applications*, 2nd ed.; Wiley: Hoboken, NJ, 2001; pp 91−92.
(45) Lefèvre, M.; Dodelet, J.-P. *Electrochim. Acta* **2003**, *48*, 2749−2760.
(46) Shen, M.-Y.; Chiao, S.-P.; Tsai, D.-S.; Wilkinson, D. P.; Jiang, J.-C. *Electrochim. Acta* **2009**, *54*, 4297−4304.
(47) Shen, M.; Scott, K. *J. Power Sources* **2005**, *148*, 24−31.



DOI: 10.1021/acscatal.5b00880
*ACS Catal.* 2015, 5, 4260−4267